Poly(ADP) ribose polymerase promotes DNA polymerase theta-mediated end joining by activation of end resection

Megan Luedeman
University of North Carolina at Chapel Hill https://orcid.org/0000-0003-3616-0770
Susanna Stroik
University of North Carolina at Chapel Hill
Wanjuan Feng
University of North Carolina at Chapel Hill
Adam Luthman
University of North Carolina at Chapel Hill
Gaorav Gupta
University of North Carolina at Chapel Hill https://orcid.org/0000-0001-9177-552X
Dale Ramsden (dale_ramsden@med.unc.edu)
UNC Chapel Hill https://orcid.org/0000-0003-1575-4748

Article

Keywords:

Posted Date: February 4th, 2022

DOI: https://doi.org/10.21203/rs.3.rs-1322147/v1

Version of Record: A version of this preprint was published at Nature Communications on August 4th, 2022. See the published version at https://doi.org/10.1038/s41467-022-32166-7.

Poly(ADP) ribose polymerase promotes DNA polymerase theta-mediated end joining by activation of end resection

Megan E Luedeman, Susanna Stroik, Wanjuan Feng, Adam J Luthman, Gaorav P Gupta, and Dale A Ramsden

Abstract

The DNA polymerase theta (Polθ)-dependent end joining (TMEJ) pathway for repair of chromosomal double strand breaks (DSBs) is essential in cells deficient in other DSB repair pathways, including hereditary breast cancers defective in homologous recombination. Strand-break activated poly(ADP) ribose polymerase 1 (PARP1) has been implicated in TMEJ, but the modest specificity of existing TMEJ assays means the extent of effect and the mechanism behind it remain unclear. We describe here a series of TMEJ assays with improved specificity and show ablation of PARP activity reduces TMEJ activity 2-4-fold. The reduction in TMEJ is attributable to a reduction in the 5' to 3' resection of DSB ends that is essential for engagement of this pathway and is compensated by increased repair by the nonhomologous-end joining pathway. This limited role for PARP activity in TMEJ helps better rationalize the combined employment of inhibitors of PARP and Polθ in cancer therapy.

Introduction

Double-strand breaks (DSBs) are repaired in mammalian cells via homologous recombination (HR), nonhomologous-end joining (NHEJ), or the still poorly understood "alternative"-end joining pathway(s) (a-EJ). Deficiencies in DSB repair lead to genome instability and cell death, and eventually, cancer or developmental disease at the organismal level[1]. Of particular importance, defects in genes important for HR (e.g. *BRCA1/2*) account for the majority of hereditary breast, ovarian, and prostate cancers[2]. Dysregulation of repair pathway choice can also contribute to disease. The choice of repair pathway is partly determined by end resection, a progressive 5' to 3' degradation of one strand of each end of the DSB that generates 3' overhanging single-stranded DNA (ssDNA) tails[1]. Resection impedes repair by NHEJ and enables repair by both HR and a-EJ[3].

It remains difficult to accurately assess repair by a-EJ pathway(s)[4]. a-EJ has historically been defined as DSB repair independent of factors required by either NHEJ and HR and is associated with an enrichment in repair products with deletions extending to sequence identities in DNA flanking the DSB (microhomologies)[5–7]. At least in mammals, the majority of repair typically associated with a-EJ utilizes microhomologies of 2-6 base pairs (bp) and is dependent on DNA polymerase theta (Polθ, encoded by *Polq*)[4,8–10]. Nevertheless, a-EJ can be detected

independent of Polθ; such repair typically requires *Helq* and longer microhomologies[4,11,12]. Here we define the subset of mammalian a-EJ missing in *Polq*-deficient cells as theta-mediated end joining (TMEJ), to distinguish it from the still unclear contribution of theta-independent a-EJ[4].

Resected end intermediates impair NHEJ but are essential for both TMEJ and HR pathways; therefore, HR-defective cells are sensitive to deficiency in, or inhibition of, Polθ (Polθi)[13–16]. The "synthetic lethality" of combined defects in HR and a second DNA repair pathway is also observed with inhibitors of poly(ADP) ribose polymerase 1 (PARP1 inhibitors; PARPi)[17,18]. Consequently, PARPi and Polθi are both being employed as therapies to target HR defective cancers. PARP1 is activated by binding to strand breaks, and it then modifies interacting proteins and itself with chains of poly(ADP) ribose (PARylation)[19]. PARPi is thought to result in dysfunctions in genome replication specifically toxic to HR-defective cancers[20–23]. The mechanisms for sensitization of HR-defective cancers to PARPi vs. Polθi are, thus, at least partly distinct, which is consistent with the additive cytotoxicity of these two inhibitors observed in HR defective cells[13,15,16].

However, interpretation of the additive effect of PARPi and Polθi is complicated by early work showing a-EJ is impaired by PARPi or deficiency in PARP1[24,25]. This role for PARP1 activity is likely unrelated to the role of PARPi in causing replication dysfunction. It seems probable that PARP deficiency or inhibition only partly impairs repair by TMEJ, or the effects of PARP1 on repair by a-EJ are wholly or partly attributable to a role for PARP1 in theta-independent a-EJ. Relevant to this latter point, inhibition of PARylation impairs recruitment of Polθ to DNA damage in cells[14,26], and PARylation of the N-terminal domain of Polθ promotes its dissociation from DNA *in vitro*[27], but it is unclear if either of these observations is sufficient to result in significant deficiency in cellular TMEJ.

Attempts to clarify the role of PARP1 in cellular TMEJ have been undercut by difficulties in unambiguously quantifying the extent of repair mediated by this pathway vs. NHEJ and theta-independent a-EJ. To resolve this concern, we developed extrachromosomal and chromosomal assays that measure TMEJ with high specificity: levels of repair detected using these assays were more than 10-fold higher in wild-type cells relative to isogenic *Polq-/-* cells. We found that deficiency in PARP signaling had no impact on TMEJ as assessed using extrachromosomal, "pre-resected" substrates. By comparison, levels of chromosomal TMEJ were reduced two to four-fold, whether using high levels of PARP inhibitor or cells deficient in PARP1 and its candidate backup, PARP2. This reduction of TMEJ levels in PARP-deficient or PARPi-treated cells paralleled decreased damage-dependent colocalization of Polθ with the resection factor CtIP, reduced levels of end resection, and finally, compensatory increases in repair by NHEJ.

Our data are consistent with an argument that PARylation does not directly impact steps specific to the TMEJ pathway. Instead, PARylation indirectly promotes Polθ recruitment and TMEJ activity at breaks by increasing the frequency of end resection and, thus, redirecting repair of these ends from NHEJ to TMEJ.

Results

Impact of PARPi on extrachromosomal and chromosomal TMEJ

The specific assessment of TMEJ activity is complicated by infrequent employment of this pathway in NHEJ proficient cells, and because the microhomology-mediated deletion products typically used as a surrogate for TMEJ are also preferential products of repair by NHEJ and theta-independent a-EJ[4]. We previously described an extrachromosomal substrate assay that emphasized repair by TMEJ, relative to NHEJ or theta-independent a-EJ, by introducing into cells linear DNA fragments with >45 nucleotide (nt) ssDNA 3'-overhangs (thus "pre-resected") with a short (4 bp) microhomology. We then exclude a contribution of NHEJ after loss of the 3' overhangs by quantifying only those repair products that retain the ssDNA overhang sequences[9,10]. Here, we additionally alter the end structure to include unpaired 5' overhangs with sequence that directs formation of an intramolecular hairpin (Fig. 1a), which helps ensure repair requires synthesis directed from 3' ssDNA tails. We also account for differences in efficiency of substrate introduction into cells by inclusion of a second extrachromosomal substrate that measures repair by NHEJ (a "spike-in control"). Repair products of these TMEJ and NHEJ substrates are then recovered from cells and measured in parallel, in a single multiplexed quantitative PCR reaction (qPCR), using 5'-nuclease probes that are specific to products of the two different repair pathways (Supplementary Fig. 1a, b). We further confirmed repair measured by the spike-in control was independent of *Polq* deficiency and PARP inhibition (10μM of olaparib) (Supplementary Fig. 1c). We performed this assay in SV40 T-antigen transformed mouse embryonic fibroblast cell lines (MEFs), comparing wild-type cells (WT) to cells derived from mice deficient in *Polq* (*Polq-/-*). Repair of the improved TMEJ substrate was not detectable in *Polq-/-* cells (Fig. 1b) and reduced 20-fold following pre-treatment of cells with 1μM of the Polθ inhibitor ART558 (Polθi). Serial dilution of products recovered from wild-type cells determined the limit of detection was <1% (>100-fold signal:noise).

We investigated the role of PARP activity in TMEJ by treating WT MEFs with vehicle (dimethyl sulfoxide; DMSO) or 10μM of the PARP inhibitor olaparib, followed by introduction of the TMEJ substrate and the NHEJ spike-in control. TMEJ activity was measured as described

above. Although this high dose of olaparib is sufficient to ablate all PARP activity[21], we see no evidence for an effect on the efficiency of TMEJ using this assay (Fig. 1b).

We considered next the possibility that TMEJ in the extrachromosomal assay is independent of PARP activity because PARP activity may have a role specific to chromosomal repair, such as chromatin remodeling or end resection. To address these possibilities, we employed a previously described chromosomal TMEJ assay, where a Cas9 nuclease guided by associated RNA generated chromosome breaks at a site in the *Rosa26* locus, after which qPCR was used to measure a microhomology-associated deletion (MHD) that was specifically depleted in *Polq*-deficient cells ($R26^{MHD}$, Fig. 2a, Supplementary Fig. 2a). In accord with previous work[9,10,28], $R26^{MHD}$ is reduced 4-fold in *Polq*-deficient contexts (either *Polq-/-* cells, or in cells pre-treated with Polθi) (Fig. 2b), relative to wild-type controls. $R26^{MHD}$ is similarly reduced upon treatment with PARPi and to a lesser extent in cells deficient in PARP1 and PARP2 (Fig. 2c, Supplementary Fig. 2b). This is consistent with a role for PARP activity in chromosomal TMEJ. However, the high background of this assay means it is not possible to definitively determine the extent of overlap between lost repair attributable to *Polq* deficiency (i.e. definitive TMEJ) and lost repair attributable to deficiency in PARylation.

We developed an assay for chromosomal TMEJ activity with greater specificity than that described above by focusing on a different class of chromosomal repair products: templated insertions (TINS). TINS are nearly unique to TMEJ, though typically less frequent and more heterogeneous than MHD products[10,29]. However, prior work from our group characterized repair at another site in the *Rosa26* locus depleted of nearby microhomologies, and consequently, TINS account for a much higher than typical fraction of TMEJ and total repair[10]. We used a qPCR designed to specifically detect TINS products at this site (Fig. 2c, Supplementary Fig. 2d; $R26^{TINS}$) and confirmed they are not detectable in *Polq-/-* cells and present at over 10-fold higher levels in isogenic *Polq*-proficient cells (Fig. 2d). Compared to cells treated with vehicle, cells treated with 10μM olaparib led to delayed accumulation of $R26^{TINS}$, eventually leading to a 39±5% reduction in accumulation of these products. A comparable reduction in $R26^{TINS}$ was observed in cells deficient in both PARP1 and PARP2 (Fig. 2e). Importantly, because $R26^{TINS}$ is entirely *Polq* dependent, our data indicate loss of PARylation impairs, but does not ablate, chromosomal TMEJ. In sum, TMEJ on a pre-resected extrachromosomal substrate is fully independent of PARylation, while PARylation activity promotes, but is not absolutely essential for, TMEJ in chromosomal contexts.

These observations are consistent with data arguing there is additive sensitivity of HR defective cells to PARPi and *Polq* loss[13,15,16] (Supplementary Fig. 3a). An additive effect on

TMEJ is also evident when using the $R26^{TINS}$ assay in cells treated with sub-saturating levels of Polθi and saturating levels of PARPi (Supplementary Fig. 3b).

Mechanism for PARP's involvement in DSB repair/TMEJ

The disparate results observed when comparing pre-resected ends (extrachromosomal assay, Fig. 1) vs. the near blunt Cas9-generated ends that require resection for TMEJ (chromosomal assays, Fig. 2) suggests the effect of PARP activity might be confined to the resection step. In agreement with previous work[14,26], inhibition of PARP reduced the frequency of Polθ foci that form after ionizing radiation (Fig. 3a, b). Here, we also observed PARP inhibition reduced the extent Polθ colocalized with an activator of resection, CTBP interacting protein (CtIP) (Mander's overlap coefficient reduced from 0.227 in vehicle-treated cells to 0.166 after treatment of cells with olaparib) (Fig. 3c, d).

We sought to directly assess if PARP inhibition affected end resection. We again introduced a targeted DSB at the *Rosa26* locus and recovered genomic DNA at various timepoints after breakage. We assessed resection near this DSB using droplet digital PCR (ddPCR), comparing mock-treated samples vs. samples treated with thermolabile Exo I, an exonuclease that specifically degrades the 3' overhanging ssDNA tails generated by end resection. 9.1±0.3% of chromosomes had a minimum of 8 nt resected, relative to the break site, 4 hours after break induction, and the frequency of ssDNA at this site declined to 2.4±0.8% by 24 hours (Fig. 4b solid black line). Over half of these ends are consistent with "short-range" resection (10 to 100 nt long ssDNA tails); a maximum of 3.8±0.4% of chromosomes had ssDNA 284 nt from the break (Supplementary Fig. S5b), and 1.7±0.5% of chromosomes had ssDNA 527 nt from the break site (Fig. 4b dashed lines). Olaparib treatment significantly reduced short-range resection – it peaked at only 5.2±0.8% of chromosomes – and the accumulation of these resected ends was slightly delayed (Fig. 4b, solid blue line). A similar impairment of short-range resection was also observed in cells deficient in PARP1 and PARP2 (Supplementary Fig. 4c). Moreover, while PARPi also impaired resection as assessed using "long-range" resection assays, the extent of impairment was less pronounced and insufficient to explain PARPi-dependent effects on TMEJ. Finally, the early reduction in resected ssDNA ends was not compensated by increased chromosomes with either dsDNA broken ends (Supplementary Fig. 5d) or deletion of both strands (Supplementary Fig. 5e).

In sum, significant effects of PARP inhibition appear confined to an impairment of short-range resection and repair by TMEJ, and apparent re-channeling to another repair fate. Consistent with this argument, an NHEJ-specific signature repair product at this locus (an insertion of a single nucleotide; reduced 50-fold in Ku-deficient cells[28]) was enriched in cells

treated with olaparib (Fig. 4d, Supplementary Fig. 2c). However, it is not possible to employ signature products to accurately estimate whether compensation is complete; thus, we sequenced all repair involving insertions and deletions (indels). We classified the TMEJ fraction as all deletions significantly reduced in *Polq-/-* cells[10] and the NHEJ fraction as all indels less than 5 bp without microhomology 2 bp or more[28] (Fig. 5a). Treatment of cells with olaparib led to reductions in the TMEJ fraction (-4.5±0.9% relative to DMSO-treated WT MEFs) that were readily accounted for by compensating increases in repair by NHEJ (4.2±1.5% relative to DMSO-treated WT MEFs; Fig. 5b). Our data indicate PARP activity promotes short-range resection and, consequently, repair by TMEJ; in the absence of PARP activity, these breaks are re-channeled to repair by NHEJ (Fig. 5c).

Discussion

Post-translational modification of proteins near strand breaks with PAR chains by PARP1 and PARP2 has diverse effects on the DNA damage response[19]. Relevant to this work, prior studies identified damage-dependent PARylation as an important promoter of the a-EJ pathway for repair of chromosome breaks[24,25]. Here, we show both inhibition of PARylation and deficiency in PARP1 and PARP2 impair end resection to a degree sufficient to explain the observed re-channeling of DSB repair from TMEJ to NHEJ (Fig. 5c). This is consistent with evidence that recruitment of Mre11, a factor important for resection, to DNA damage is impaired in the absence of PARylation,[30,31] as well as our demonstration that inhibition of PARylation reduces ionizing-radiation-dependent colocalization of CtIP (also required for resection) and Polθ (Fig. 3d). We also see no evidence for effects of PARylation on TMEJ when this pathway is assessed independent of resection (i.e., in repair of pre-resected ends; Fig. 1). The PARP-dependent effects on resection and channeling to TMEJ observed here is consistent with prior observations that recruitment of PARP1 and the NHEJ factor Ku are mutually exclusive[25,31,32].

Prior evidence on the role of PARP activity in regulation of long-range resection, as well as recruitment of factors required for long-range resection (EXO1) has been contradictory[33–37]. Here we observe that levels of long-range resection (>284 nucleotides), as well as the effects of PARP inhibition on long-range resection (mildly inhibitory) are of insufficient magnitude to explain the influence of PARPi on DSB repair pathway choice.

Taken together, our data are consistent with a model in which PARP1 instead of Ku is recruited to a minor subset of DSBs. The resulting activation of local PARylation facilitates i) recruitment of factors (Mre11, Rad50, Nbs1, CtIP) important for short-range resection, ii) generation of the 20-100 nt, 3’ ssDNA overhangs that are preferential substrates for Polθ/TMEJ, iii) recruitment of Polθ, and iv) repair by TMEJ instead of NHEJ (Fig. 5c). The observed PAR-

mediated increased recruitment of Polθ at breaks[14,26] (Fig. 3b) may be an indirect consequence of PAR-dependent effects on resection. Additionally, the lack of a role for PARylation observed when TMEJ is measured using extrachromosomal, pre-resected substrates argues against a significant direct role for PARylation in promoting TMEJ after resection has been initiated. Of note, confinement of the role of PARPi to regulation of resection would argue it could also impact Theta-independent a-EJ (Fig. 5c), an interpretation consistent with the slight ability of olaparib to deplete non-NHEJ products in *Polq-/-* cells (compare depleted products in last two columns; Fig. 5b).

Resection and TMEJ are reduced to a greater degree when cells are treated with PARP inhibitors, relative to that observed in PARP deficient cells, though this difference is typically modest and not always statistically significant. The ability of PARP inhibitors to delay disassociation of PARP1 at ends ("trapping")[21] may interfere with the ability of the resection machinery to access DNA ends, eventually leading to a redirection of the repair of these ends to NHEJ.

TMEJ was only modestly impaired (reduced 2-4-fold) by deficiency in both PARP1 and PARP2, as well as by treatment of cells with saturating levels of PARPi. The remaining TMEJ activity in PARP inhibited cells was also sensitive to treatment with Polθi even when using sub-saturating concentrations of Polθi. This incomplete epistasis – the observation that even fully ablated PARylation activity only modestly impairs TMEJ activity – explains why the toxicity of PARPi and Polθi is additive in HR-deficient cancers, and better rationalizes the utility of combined therapy.

The specific toxicity of PARPi in HR defective cancers is primarily attributed to the ability of PARPi to generate replication fork dysfunctions that preferentially engage HR[20–23]. Our data suggest the ability of PARPi to impair resection could also exacerbate the original HR defect, providing an independent mechanism for specific toxicity (Fig. 5c). That deficiency in an antagonist of resection, 53BP1, promotes resistance to PARPi in HR defective cancers[38,39] is also consistent with this argument since increased resection due to 53BP1 loss would similarly help mitigate the ability of PARPi to impair resection. Our observations thus further expand the links between factors that regulate end resection and the determinants of therapeutic response in HR defective cancers.

Materials and Methods

Materials

Olaparib was purchased from Selleck Chemicals, ART558 was provided by Artios Pharma Limited, and both were dissolved in dimethyl sulfoxide (DMSO, Sigma).

Cell lines

All cell lines were cultured at 37°C and 5% CO_2 and confirmed to be free of mycoplasma contamination by PCR (detection limit less than 10 genomes/mL). Mouse embryonic fibroblasts (MEFs) were plated in DMEM (Corning) containing 10% Fetal Bovine Serum (VWR Life Sciences, Seradigm) and penicillin (5U/mL, Sigma). MEFs were SV40 T-antigen transformed cells derived from mice proficient (wild type; WT) or deficient in *Polq* (*Polq-/-*) and were previously characterized[8]. Variant clones of the WT MEFs deficient in *Parp1* (*Parp1-/-*) were generated using Cas9 and the guide listed in Supplementary Table 1; *Parp2* deficiency was generated in a *Parp1-/-* clonal line by a subsequent introduction of Cas9 and the guide listed in Supplementary Table 1 to generate a clonal line deficient in *Parp1* and *Parp2* (*Parp1/2-/-*). Retinal pigment epithelial (RPE-1) cells immortalized by human telomerase reverse transcriptase (hTERT) expression were cultured in DMEM F12 (Invitrogen) containing 10% Fetal Bovine Serum (VWR Life Sciences, Seradigm) and penicillin (5U/mL, Sigma). A clonal HALO-tagged POLQ line was derived from retroviral transduction of a HALO-POLQ construct (a gift from Richard Wood). *Brca1/p53* null KPB13 murine mammary tumor cells were previously characterized[40,41] and plated in HuMEC with 5% Fetal Bovine Serum (VWR Life Sciences, Seradigm), penicillin (5U/mL, Sigma), and the HuMEC (Gibco) supplementary kit (Gibco). A clonal line stably expressing human *BRCA1* was generated by transfer of the cDNA from Addgene 52504 to pEZY3 (Addgene #18672), linearization, and selection for clones with expression as confirmed by RT-qPCR. Variant clones of the parental KPB13 line deficient in *Polq* were generated using Cas9 and the guides listed in Supplementary Table 1.

Extrachromosomal assay

Synthetic DNA for extrachromosomal substrates were purchased from IDT (ultramers; sequences in Supplementary Table 2) and annealed using a thermocycler (Applied Biosystems) in a buffer containing 10mM Tris-HCL pH 7.5, 100mM NaCl, and 0.1mM EDTA. 500ng of the TMEJ substrate, 20ng of the NHEJ substrate, and 1µg of pMAX-GFP (Lonza) were electroporated into 200,000 cells with a single 1,350 V, 30 ms pulse using the Neon system (Invitrogen). Cells were pre-treated for two hours with media supplemented with the indicated concentrations of olaparib, ART558, or vehicle (DMSO) prior to electroporation and then incubated in supplemented media again for 30 minutes post electroporation. Cells were washed with 1x Dulbecco's phosphate-buffered solution (DPBS; Gibco) and then incubated at 37°C for 10 minutes in Hank's balanced saline solution containing 25U of Benzonase (Sigma). The QIAamp DNA mini kit (QIAGEN) was used to purify DNA and samples were analyzed using qPCR with TaqMan Fast Advanced Master Mix (Applied Biosystems; primers and probes

described in Supplementary Table 3). Extrachromosomal TMEJ and NHEJ PCR efficiencies, their independence from each other, and their limits of detection (LOD) were determined by diluting a synthetic DNA containing the extrachromosomal TMEJ or NHEJ amplicon (IDT) into genomic DNA containing constant amounts of the other amplicon sequence (Supplementary Fig. 1a, b). NHEJ joining efficiencies were used to adjust TMEJ efficiencies for each replicate. Experiments consisted of three replicates of the electroporation.

Chromosomal qPCR assays

CRISPR RNAs (crRNAs) specific for sites in the Rosa26 locus are described in Supplementary Table 4. For generating chromosomal DSBs targeted to these sites, 7 pmol of Cas9 was incubated with 8.4 pmol of annealed crRNA+tracrRNA (Alt-R, IDT) at room temperature for 30 mins, then mixed with 32 ng of pMAX-GFP before electroporation of the mixture into 200,000 cells as described above. Two electroporations were pooled for each replicate. Cells were treated with media supplemented with the indicated drug concentrations or DMSO overnight and then plated into media containing fresh drug or DMSO after electroporation. DNA was extracted from cells at indicated time points using a QIAamp DNA mini kit (QIAGEN). Signature repair products were measured via qPCR using 50ng of DNA with TaqMan Fast Advanced Master Mix (Applied Biosystems; primers and probes described in Supplementary Table 3). A linear response to decreasing template and LODs were confirmed by diluting DNA from a Cas9-cut, WT DMSO sample recovered 24 ($R26^{MHD}$ and R26 NHEJ) or 48 ($R26^{TINS}$) hours after Cas9 introduction to cells into unbroken genomic DNA (Supplementary Fig. S2a, c and d). All signature qPCRs were normalized to a reference amplicon 32kb downstream of the Cas9-cut site (Ref2) as measured in an independent PCR reaction.

Immunoblotting

Whole cell lysates were generated using radioimmunoprecipitation assay (RIPA) buffer with freshly added phosphatase (Sigma, P0044) and protease inhibitors (Sigma, P8340). 50µg of lysate in sodium dodecyl sulphate (SDS)-loading buffer was loaded onto 8% tris-glycine SDS polyacrylamide gels. Proteins were transferred to a nitrocellulose membrane (General Electric) in tris-glycine transfer buffer containing 20% methanol. Membranes were blocked in 5% fat-free milk (Carnation) for 1 hour at room temperature, and then incubated overnight at 4°C in primary antibody (PARP1 Enzo ALX-210-302-R100; PARP2 Enzo ALX-210-899-R100; Actin Novus NB600-535) diluted in phosphate buffered solution with 0.1% Tween-20 (PBST), and then in secondary antibodies (LI-COR) diluted 1:10,000 in PBST for 1 hour at room temperature. Membranes were imaged on a Licor Odessey.

Clonogenic Survival Assay

KPB13 cells were plated in triplicates for each condition, 1,000 cells per 10 cm dish, with 10 ml growth media. Olaparib was added the next day after cell seeding to the final concentrations of 0.1 μM or 0.3 μM. Cells were harvested for crystal violet staining and colony counting seven to ten days later. The clonogenic surviving fraction was determined as the ratio between the plating efficiency of treated versus untreated cells.

Immunofluorescence

HALO-POLQ expressing RPE-1 cells were plated at 70% density on chamber slides 24 hours prior to treatment. Vehicle or olaparib was added immediately prior to irradiation with 10Gy in a RadSource RS2000 irradiator. Cells recovered for two hours post-irradiation prior to harvest. Janelia Fluor 549 HaloTag Ligand (Promega) was added to the recovery media 15 minutes prior to collection. Upon collection, cells were fixed with 4% paraformaldehyde (Electron Microscopy Services) and permeabilized with 0.5% Nonidet P-40 substitute (Fluka). The cells were then blocked with 0.5% BSA (Fisher Bioreagents) and 0.2% fish gelatin (Sigma) prior to primary antibody incubation in blocking solution overnight. Primary antibodies used were anti-CtIP (Novus; NB-79610) and anti-gamma H2AX (Cell Signaling Technology; 9718). Slides were then washed and incubated with Alexa Fluor secondary antibodies in blocking solution. Cells were subsequently washed and stained with DAPI (BioLegend) prior to mounting. Images were acquired on a BX61 Olympus microscopy with recommended Z stack depth optimization. Images were processed with Imaris and FIJI software packages.

Droplet Digital PCR

Chromosomal DSBs were induced as described above for the chromosomal qPCR assays using the $R26^{MHD}$ crRNA, and DNA was extracted at the listed time points using QIAamp DNA mini kit (QIAGEN). Samples were digested with NdeI (New England Biolabs; NEB) and either incubated with 50% glycerol (mock-treated; Sigma) or 20 units Thermolabile Exonuclease I (ExoI-treated; NEB) at 37°C for 2 hours in a buffer containing 10mM Tris-HCl, 50mM KCl, and 1.5mM $MgCl_2$. All samples were heated to 65°C for 5 minutes to inactivate ExoI. Droplet Digital PCR (ddPCR) was performed with 25ng of digested DNA and ddPCR Supermix for Probes (no dUTP) (BioRad Laboratories). Droplets were generated and read using the QX200 AutoDG Droplet Digital PCR System (BioRad Laboratories). TMEJ and NHEJ signatures were measured and normalized using the same primers and probes as described in the chromosomal qPCR assays. We confirmed for the Ref1 and Flank amplicons that amplification was linear in response to the amount of template and independent of multiplexed amplicon amplification efficiency (e.g. Supplementary Figure 4a, b); we similarly confirmed the “Intact” target amplicon was linear in response to the fraction of broken DNA by serial dilution of XbaI (NEB) digested

genomic DNA (XbaI cuts immediate adjacent to Cas9-target site) into unbroken genomic DNA (Supplementary Fig. 4c, green circles). We further confirmed Exo I digestion conditions were specific for ssDNA ends (does not degrade XbaI-generated dsDNA ends; Supplementary Figure 4c black x's, Supplementary Table 5) and able to fully degrade ssDNA ends using a spike-in ssDNA control (Supplementary Figure 4d, e, Supplementary Table 5). The fraction of ssDNA (Exo I-sensitive amplification) and deletions >8bp, >284bp, and >527bp were determined using an amplicon ending 7bp, 283bp, and 526bp, respectively, upstream of the Cas9-cut site (flank; Fig. 4a). The minimum length of ssDNA/deletion was determined by the amplification efficiency of synthetic DNAs with progressively increased deletion of the sequence proximal to the break site. The sequence of all primers, probes, and synthetic DNA controls used can be found in Supplementary Table 3.

Next-generation sequencing library preparation

Chromosomal DSBs and DNA extraction were performed as in the chromosomal assays. Polyacrylamide gel electrophoresis-purified primers (IDT) containing a 6 bp barcode, a spacer sequence of varying length (1-8 bp) to increase library diversity, and 21 (Fwd primer) or 22 (Rev primer) bp of Illumina adapter sequence (sequences in Supplementary Table 6) were used to amplify DNA equivalent to 60,000 genomes for 24 cycles. Libraries were purified with a 2% agarose (Lonza) gel and the QIAquick Gel Extraction Kit (QIAGEN), and then the recovered DNA was amplified for five cycles using secondary NGS PCR primers (Supplementary Table 6) and purified using AMPure XP beads (Beckman Coulter). Libraries were sequenced using an Illumina iSeq 100 i1 kit (300-cycle) with 20% PhiX Control v3 DNA (Illumina).

High-throughput sequencing junction characterization

The total number of reads generated and analyzed per sample are listed Table S7. Data were analyzed using CLC Genomic Workbench 8 as previously described[10] and junctions were characterized using a custom Python script (PyCharm Community Edition 2021, JetBrains) as outlined here. Junctions were scanned for matches of 10 nucleotides, starting proximal to the break site and searching for an upstream and downstream match corresponding to the smallest possible deletion. These matches established deletion length to the left and right, respectively. Junctions were then reconstructed as the sequence between the 5' end of the upstream match and the 3' end of the downstream match. Junctions were further characterized for insertions (any intervening sequence between the left and right 10 nucleotide matches) and microhomologies (sequence overlap between the left and right 10 nucleotide matches). We excluded junctions containing base ambiguities (i.e. N, W, S, R, K) and junctions with base substitutions in the 3-10 nucleotides proximal to the break site if nucleotides adjacent to the

substitution matched the corresponding reference sequence; these substitutions are consistent with polymerase error during sample amplification and are misattributed as insertions. Deletions significantly depleted in *Polq-/-* MEFs identified via the Benjamini-Hochberg procedure[42] were categorized as TMEJ[10]. Sequences with insertions or deletions <5 bp and MH<2 bp were characterized as NHEJ[28], and all other sequences (insertions or deletions ≥5 bp not dependent on *Polq*), were listed as other.

Statistical analysis

The number of replicates and statistical tests are listed with figures and were conducted using GraphPad Prism 9, and all p values determined by ANOVA were corrected for multiple comparisons. Statistical tests were run on cycle threshold (C_t) values for all qPCR data, before transformation of data for the linear scale representations in display figures. The Benjamini-Hochberg procedure[42] was used to identify products depleted in *Polq*-deficient cells (Figure 5b) in Microsoft Excel with a false discovery rate of 10%.

Data availability

All raw fastq files will be available at NCBI SRA upon acceptance. All other data will be made available upon request.

References

1. Scully, R., Panday, A., Elango, R. & Willis, N. A. DNA double-strand break pathway choice in somatic mammalian cells. *Nat. Rev. Mol. Cell Biol.* **20**, 698–714 (2019).
2. King, M. C., Marks, J. H. & Mandell, J. B. Breast and ovarian cancer risks due to inherited mutations in BRCA1 and BRCA2. *Science* **302**, 643–646 (2003).
3. Symington, L. S. & Gautier, J. Double-Strand Break End Resection and Repair Pathway Choice. *Annu. Rev. Genet.* **45**, 247–271 (2011).
4. Ramsden, D. A., Carvajal-Garcia, J. & Gupta, G. P. Mechanism, cellular functions and cancer roles of polymerase-theta-mediated DNA end joining. *Nat. Rev. Mol. Cell Biol.* **23**, 125–140 (2022).
5. Boulton, S. J. & Jackson, S. P. *Saccharomyces cerevisiae* Ku70 potentiates illegitimate DNA double-strand break repair and serves as a barrier to error-prone DNA repair pathways. *EMBO J.* **15**, 5093–5103 (1996).
6. Kabotyanski, E. B., Gomelsky, L., Han, J., Stamato, T. D. & Roth, D. B. Double-strand break repair in Ku86- and XRCC4-deficient cells. *Nucleic Acids Res.* **26**, 27–31 (1998).
7. Liang, F. & Jasin, M. Ku80-deficient Cells Exhibit Excess Degradation of Extrachromosomal DNA. *J. Biol. Chem.* **271**, 14405–14411 (1996).
8. Yousefzadeh, M. J. *et al.* Mechanism of Suppression of Chromosomal Instability by DNA

Polymerase POLQ. *PLoS Genet.* **10**, (2014).
9. Wyatt, D. W. *et al.* Essential Roles for Polymerase θ-Mediated End Joining in the Repair of Chromosome Breaks. *Mol. Cell* **63**, 662–673 (2016).
10. Carvajal-Garcia, J. *et al.* Mechanistic basis for microhomology identification and genome scarring by polymerase theta. *PNAS* **117**, 8476–8485 (2020).
11. Kamp, J. A. *et al.* Helicase Q promotes homology-driven DNA double-strand break repair and prevents tandem duplications. *Nat. Commun.* **12**, (2021).
12. Anand, R. *et al.* HELQ is a dual-function DSB repair enzyme modulated by RPA and RAD51. *Nature* **51**, (2021).
13. Ceccaldi, R. *et al.* Homologous-recombination-deficient tumours are dependent on Polθ -mediated repair. *Nature* **518**, 258–262 (2015).
14. Mateos-Gomez, P. A. *et al.* Mammalian polymerase θ promotes alternative NHEJ and suppresses recombination. *Nature* **518**, 254–257 (2015).
15. Zatreanu, D. *et al.* Polθ inhibitors elicit BRCA-gene synthetic lethality and target PARP inhibitor resistance. *Nat. Commun.* **12**, (2021).
16. Zhou, J. *et al.* A first-in-class Polymerase Theta Inhibitor selectively targets Homologous-Recombination-Deficient Tumors. *Nat. Cancer* **2**, 598–610 (2021).
17. Farmer, H. *et al.* Targeting the DNA repair defect in BRCA mutant cells as a therapeutic strategy. *Nat. Cell Biol.* **434**, 917–921 (2005).
18. Bryant, H. E. *et al.* Specific killing of BRCA2-deficient tumours with inhibitors of poly (ADP-ribose) polymerase. *Nature* **7**, 913–918 (2005).
19. Chaudhuri, A. R. & Nussenzweig, A. The multifaceted roles of PARP1 in DNA repair and chromatin remodelling. *Nat. Publ. Gr.* **18**, 610–621 (2017).
20. Maya-Mendoza, A. *et al.* High speed of fork progression induces DNA replication stress and genomic instability. *Nature* **559**, 279–284 (2018).
21. Murai, J. *et al.* Trapping of PARP1 and PARP2 by clinical PARP inhibitors. *Cancer Res.* **72**, 5588–5599 (2012).
22. Hanzlikova, H. *et al.* The Importance of Poly (ADP-Ribose) Polymerase as a Sensor of Unligated Okazaki Fragments during DNA Replication Article The Importance of Poly (ADP-Ribose) Polymerase as a Sensor of Unligated Okazaki Fragments during DNA Replication. *Mol. Cell* **71**, 319–331 (2018).
23. Cong, K. *et al.* Replication gaps are a key determinant of PARP inhibitor synthetic lethality with BRCA deficiency. *Mol. Cell* **81**, 3128–3144 (2021).
24. Audebert, M., Salles, B. & Calsou, P. Involvement of poly(ADP-ribose) polymerase-1 and

XRCC1/DNA ligase III in an alternative route for DNA double-strand breaks rejoining. *J. Biol. Chem.* **279**, 55117–55126 (2004).

25. Wang, M. *et al.* PARP-1 and Ku compete for repair of DNA double strand breaks by distinct NHEJ pathways. *Nucleic Acids Res.* **34**, 6170–6182 (2006).
26. Kais, Z. *et al.* FANCD2 Maintains Fork Stability in BRCA1/2- Deficient Tumors and Promotes Alternative End- Joining DNA Repair. *CellReports* **15**, 2488–2499 (2016).
27. Schaub, J. M., Soniat, M. M. & Finkelstein, I. J. Polymerase theta-helicase promotes end joining by stripping single-stranded DNA-binding proteins and bridging DNA ends. *BioRxiv* 1–9 (2021).
28. Feng, W. *et al.* Marker-free quantification of repair pathway utilization at Cas9-induced double-strand breaks. *Nucleic Acids Res.* **49**, 5095–5105 (2021).
29. Schimmel, J., Schendel, R. Van, Dunnen, J. T. Den & Tijsterman, M. Templated Insertions : A Smoking Gun for Polymerase Theta-Mediated End Joining. *Trends Genet.* **35**, 632–644
30. Haince, J. F. *et al.* PARP1-dependent kinetics of recruitment of MRE11 and NBS1 proteins to multiple DNA damage sites. *J. Biol. Chem.* **283**, 1197–1208 (2008).
31. Cheng, Q. *et al.* Ku counteracts mobilization of PARP1 and MRN in chromatin damaged with DNA double-strand breaks. *Nucleic Acids Res.* **39**, 9605–9619 (2011).
32. Yang, G. *et al.* Super-resolution imaging identifies PARP1 and the Ku complex acting as DNA double-strand break sensors. *Nucleic Acids Res.* **46**, 3446–3457 (2018).
33. Caron, M. *et al.* Poly(ADP-ribose) polymerase-1 antagonizes DNA resection at double-strand breaks. *Nat. Commun.* **10**, (2019).
34. Zhang, F., Shi, J., Bian, C. & Yu, X. Poly(ADP-Ribose) Mediates the BRCA2-Dependent Early DNA Damage Response. *Cell Rep.* **13**, 678–689 (2015).
35. Chen, S.-H., Bian, C., Yu, X., Zhang, F. & Shi, J. The PIN domain of EXO1 recognizes poly(ADP-ribose) in DNA damage response. *Nucleic Acids Res.* **43**, 10782–10794 (2015).
36. Liu, T. & Huang, J. DNA End Resection: Facts and Mechanisms. *Genomics, Proteomics Bioinforma.* **14**, 126–130 (2016).
37. Cheruiyot, A. *et al.* Poly (ADP-ribose) -binding promotes Exo1 damage recruitment and suppresses its nuclease activities. *DNA Repair* **35**, 106–115 (2015).
38. Bunting, S. F. *et al.* 53BP1 inhibits homologous recombination in Brca1-deficient cells by blocking resection of DNA breaks. *Cell* **141**, 243–254 (2010).
39. Bouwman, P. *et al.* 53BP1 loss rescues BRCA1 deficiency and is associated with triple-

negative and BRCA-mutated breast cancers. *Nat. Struct. Mol. Biol.* **17**, 688–695 (2010).
40. Liu, X. *et al.* Somatic loss of BRCA1 and p53 in mice induces mammary tumors with features of human BRCA1-mutated basal-like breast cancer. *Proc. Natl. Acad. Sci. U. S. A.* **104**, 12111–12116 (2007).
41. Hollern, D. P. *et al.* A mouse model featuring tissue-specific deletion of p53 and Brca1 gives rise to mammary tumors with genomic and transcriptomic similarities to human basal-like breast cancer. *Breast Cancer Res. Treat.* **174**, 143–155 (2019).
42. Ferreira, J. A. & Zwinderman, A. H. On the benjamini–hochberg method. *Ann. Stat.* **34**, 1827–1849 (2006).

Acknowledgements

We would like to thank Artios Pharma Limited for supplying ART-558, Dr. Rick Wood for providing the WT and *Polq-/-* MEFs, and Marianna Jones for generating the *Parp1-/-* MEFs. This work was supported by the US DOD grant W81XWH18-1-0046 and the US NIH grant P01CA247773 to D.A.R. and G.P.G. M.E.L. was supported by the US NIGMS grant 5T32 GM007092. S.S. is supported by the US NCI grant F32CA264891. A.J.L. was supported by T32 GM119999.

Author Information

Affiliations

Curriculum in Genetics and Molecular Biology, University of North Carolina at Chapel Hill, Chapel Hill, NC, USA

Megan E. Luedeman, Gaorav P. Gupta, and Dale A. Ramsden

Lineberger Comprehensive Cancer Center, University of North Carolina at Chapel Hill, Chapel Hill, NC, USA

Susanna Stroik, Wanjuan Feng, Gaorav P. Gupta, and Dale A. Ramsden

Department of Biochemistry and Biophysics, University of North Carolina at Chapel Hill, Chapel Hill, NC, USA

Adam J. Luthman, Gaorav P. Gupta, and Dale A. Ramsden

Department of Radiation Oncology, University of North Carolina at Chapel Hill, Chapel Hill, NC, USA

Gaorav P. Gupta

Contributions

Generated and analyzed data and/or developed methodology: all authors. Drafted the manuscript: M.E.L. and D.A.R. Edited and approved the final manuscript: all authors. Conceptualization of the study: M.E.L. and D.A.R.

Corresponding Author

Dale A. Ramsden

Competing Interests

G.P.G. receives research funding from Breakpoint Therapeutics, which is developing inhibitors of Polθ. D.A.R. has a materials transfer agreement with Artios Pharma and is using an Artios Pharma compound that inhibits Polθ for research purposes with no financial compensation.

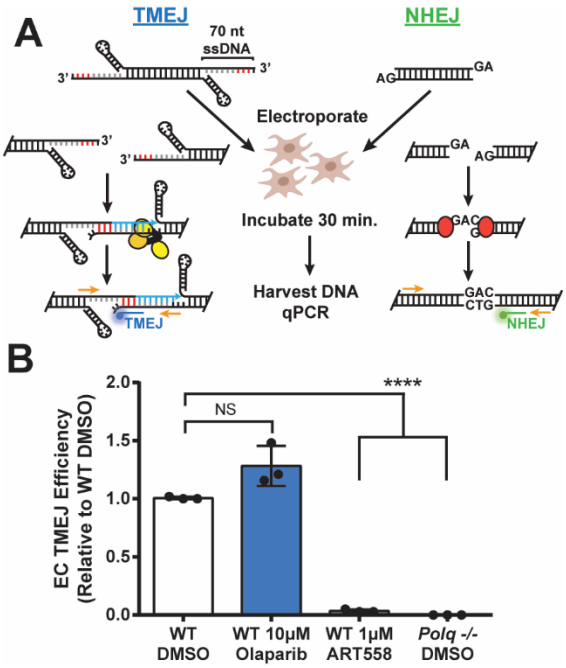

519

520 **Figure 1 PARPi does not impact extrachromosomal TMEJ**

521 **A)** Schematic of the extrachromosomal assay (EC) and pathway-specific probe qPCR (orange
522 primers with blue TMEJ and green NHEJ probes). The microhomology in the TMEJ substrate is
523 shown in red and Polq-dependent synthesis in blue. **B)** TMEJ substrate joining efficiency,
524 normalized with NHEJ substrate joining efficiency to account for differences in transfection
525 efficiency, is expressed as a fraction of the TMEJ observed in wild-type MEFs treated with
526 vehicle (WT DMSO). Data shown are mean ± standard deviation (SD) (n=3). Statistical
527 significance of differences, relative to WT DMSO cells, was determined by one-way ANOVA
528 (****p<0.0001, NS, not significant).

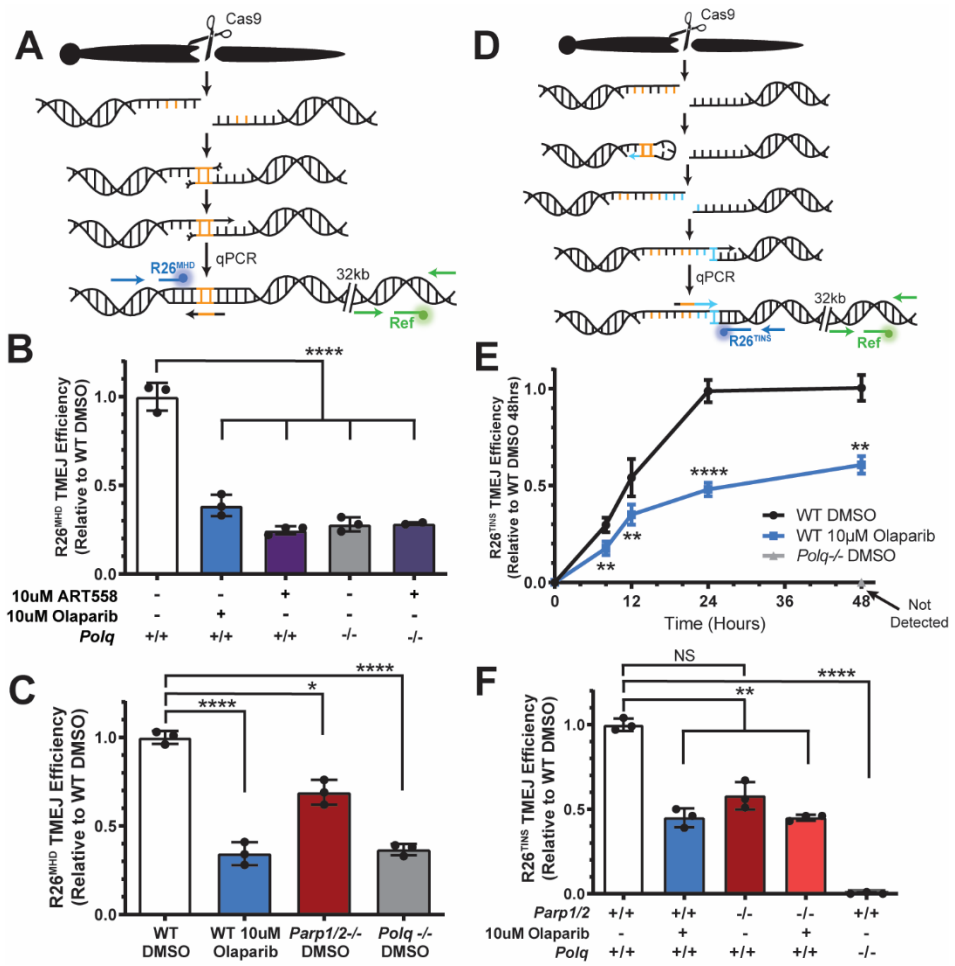

Figure 2 Loss of PARP activity partially inhibits chromosomal TMEJ

A) Model of the formation of the microhomology (orange) mediated deletion signature TMEJ repair product ($R26^{MHD}$) and its detection by qPCR. The location of primers and probe is identified for the $R26^{MHD}$ amplicon in blue and the reference amplicon in green. **B and C)** $R26^{MHD}$ TMEJ efficiency after 24 hours comparing DMSO-treated WT or *Polq-/-* MEFs to MEFs treated with olaparib or ART558 (**B**) or *Parp1/2-/-* MEFs (**C**). **D)** Model of the formation of the templated insertion (blue section) signature TMEJ repair product ($R26^{TINS}$) and its detection by qPCR. The location of primers and probe is identified for the $R26^{TINS}$ amplicon in blue and the reference amplicon in green. **E)** Accumulation of the $R26^{TINS}$ TMEJ signature over 48 hours in WT MEFs treated with DMSO (black) or 10μM olaparib (blue). *Polq-/-* MEFs had no detectable signal (grey). **F)** $R26^{TINS}$ TMEJ efficiency after 48 hours in WT, *Parp1/2-/-*, and *Polq-/-* MEFs treated with DMSO or 10μM olaparib. All signatures are normalized to the number of genomes as determined by a reference (Ref) amplicon 32 kilobases (kb) downstream and are expressed as a fraction of that observed in WT cells treated with DMSO. All data shown are mean ± SD

(n=3), and statistical significance of differences, relative to WT DMSO cells, was determined by one-way ANOVA (*p<0.05, **p<0.01, ****p<0.0001, NS, not significant).

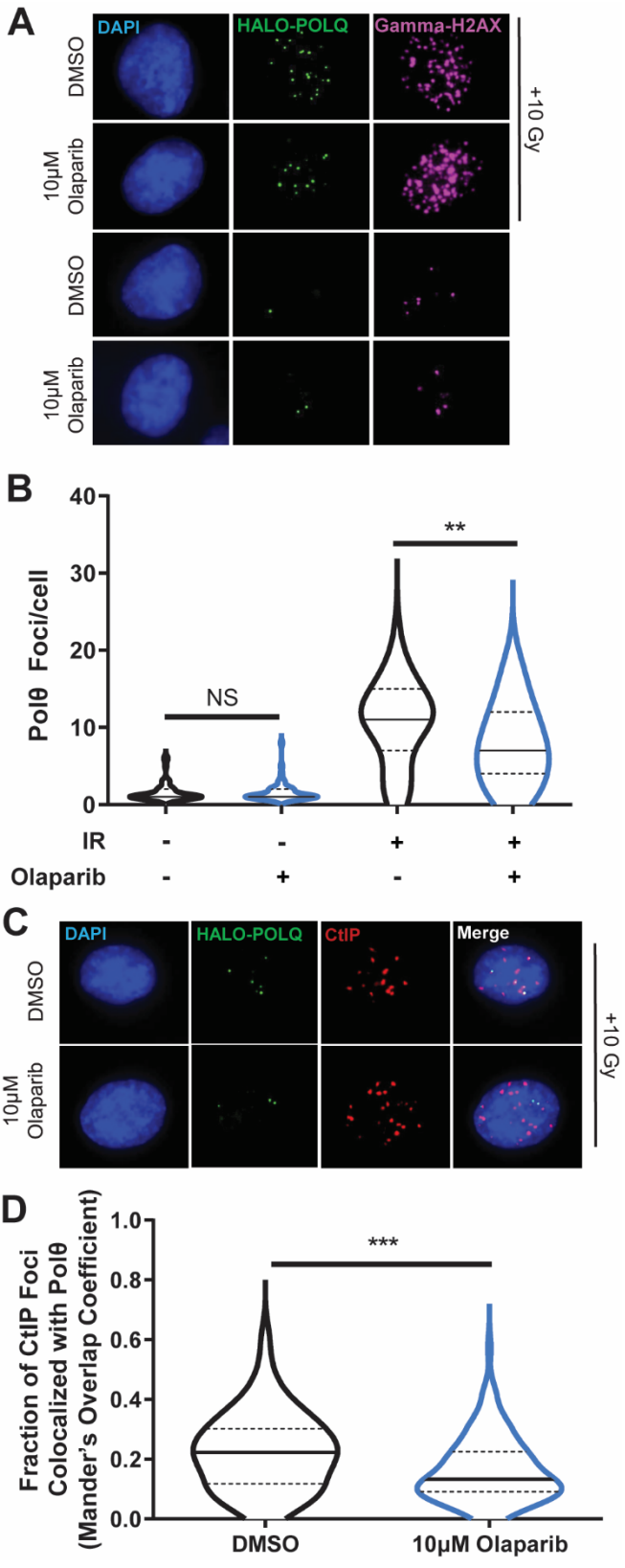
A
DAPI
HALO-POLQ
Gamma-H2AX
DMSO
10μM Olaparib
DMSO
10μM Olaparib
+10 Gy
B
Polθ Foci/cell
40
30
20
10
0
**
NS
IR
-
-
+
+
Olaparib
-
+
-
+
C
DAPI
HALO-POLQ
CtIP
Merge
DMSO
10μM Olaparib
+10 Gy
D
Fraction of CtIP Foci Colocalized with Polθ (Mander's Overlap Coefficient)
1.0
0.8
0.6
0.4
0.2
0.0
***
DMSO
10μM Olaparib

Figure 3 PARP activity promotes Polθ foci formation and colocalization with CtIP

A) Representative images of HALO-POLQ foci (green) in DMSO- or olaparib-treated RPE-1 cells without damage or with damage induced by 10 Gray (Gy) of ionizing radiation (IR). DAPI (blue) marks nuclei, and GammaH2AX (pink) indicates damage. **B)** Number of Polθ foci per cell in cells with >0 foci (DMSO+IR n = 55, olaparib+IR n = 43, DMSO n=50, olaparib n=50). Significance of difference determined by one-way ANOVA (**p<0.01, NS, not significant). The distribution of foci/cell is represented by a truncated violin plot including median (solid line) and upper and lower quartile (dashed lines) values. **C)** Representative images of HALO-POLQ (green) and CtIP (red) foci in irradiated RPE-1 cells. **D)** Fraction of CtIP foci colocalized with Polθ (Mander's overlap coefficients; DMSO n=100, olaparib n=100). Significance of difference determined by unpaired t-test (***p<0.001). The distribution of foci/cell is represented by a truncated violin plot including median (solid line) and upper and lower quartiles (dashed lines) values.

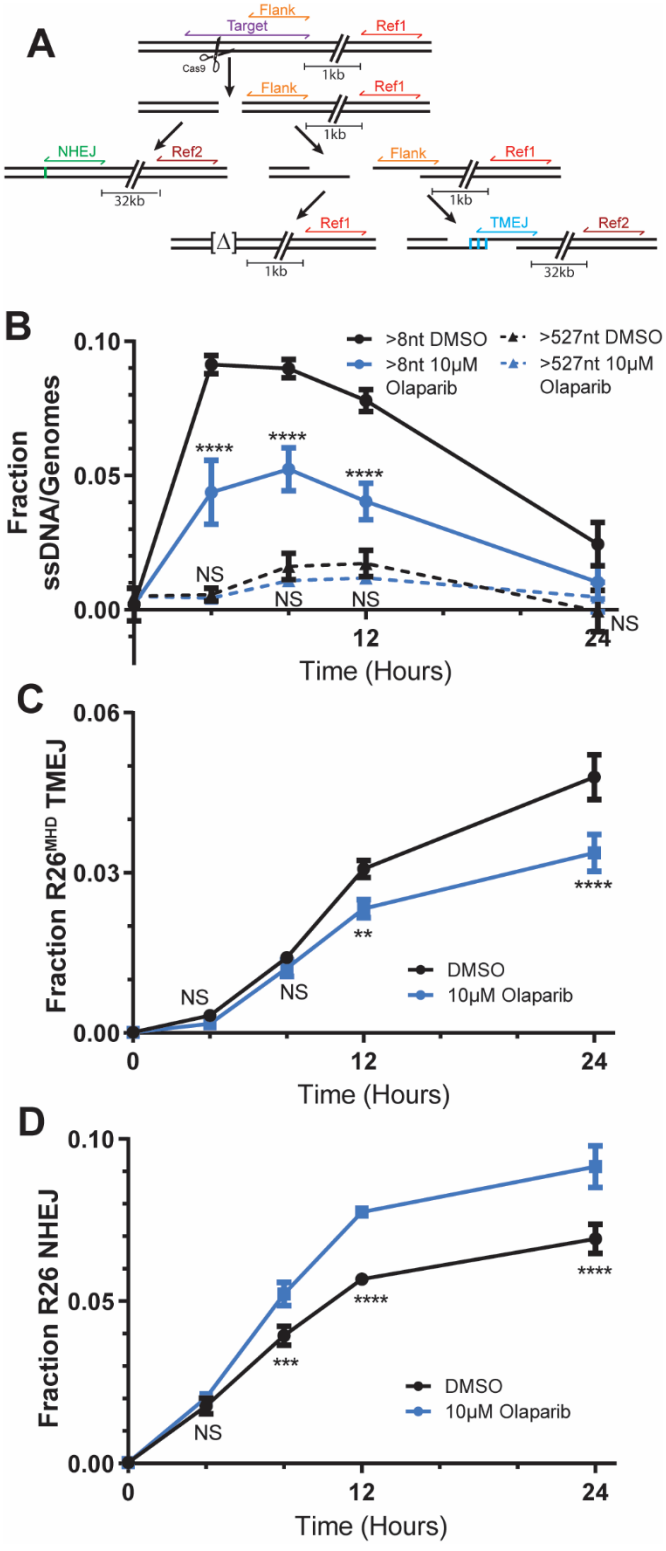
A
Flank
Target
Ref1
Cas9
1kb
NHEJ
Ref2
32kb
[Δ]
TMEJ
B
>8nt DMSO
>8nt 10μM Olaparib
>527nt DMSO
>527nt 10μM Olaparib
Fraction ssDNA/Genomes
0.10
0.05
0.00
****
NS
12
24
Time (Hours)
C
Fraction R26MHD TMEJ
0.06
0.03
0.00
**
DMSO
10μM Olaparib
0
Time (Hours)
D
Fraction R26 NHEJ
***

Figure 4 Loss of PARP activity inhibits resection and promotes NHEJ

A) Diagram depicting repair intermediates and outcomes of a Cas9-induced DSB. Amplicons used for ddPCR are shown in color; Δ indicates deletion repair products. The number of genomes in each PCR was determined by a reference amplicon ~1kb (Ref1) or ~32kb (Ref2) from the cut site. **B)** Fraction of genomes with ssDNA >8nt (solid lines) or >527nt (dashed lines) generated by 5'-to-3' resection in WT MEFs treated with DMSO (black) or 10μM olaparib (blue) over 24 hours. **C)** Fraction of genomes repaired by $R26^{MHD}$ TMEJ signature or **D)** R26 NHEJ signature in WT MEFs treated with DMSO (black) or 10μM olaparib (blue) over 24 hours. Data shown are mean ± SD of one biological replicate and four technical replicates; the same biological replicate was used in B-D. Statistical significance of differences, relative to WT DMSO cells, was determined by one-way ANOVA (*p<0.05, **p<0.01, ***p<0.001, ****p<0.0001). See also Supplementary Fig. 5.

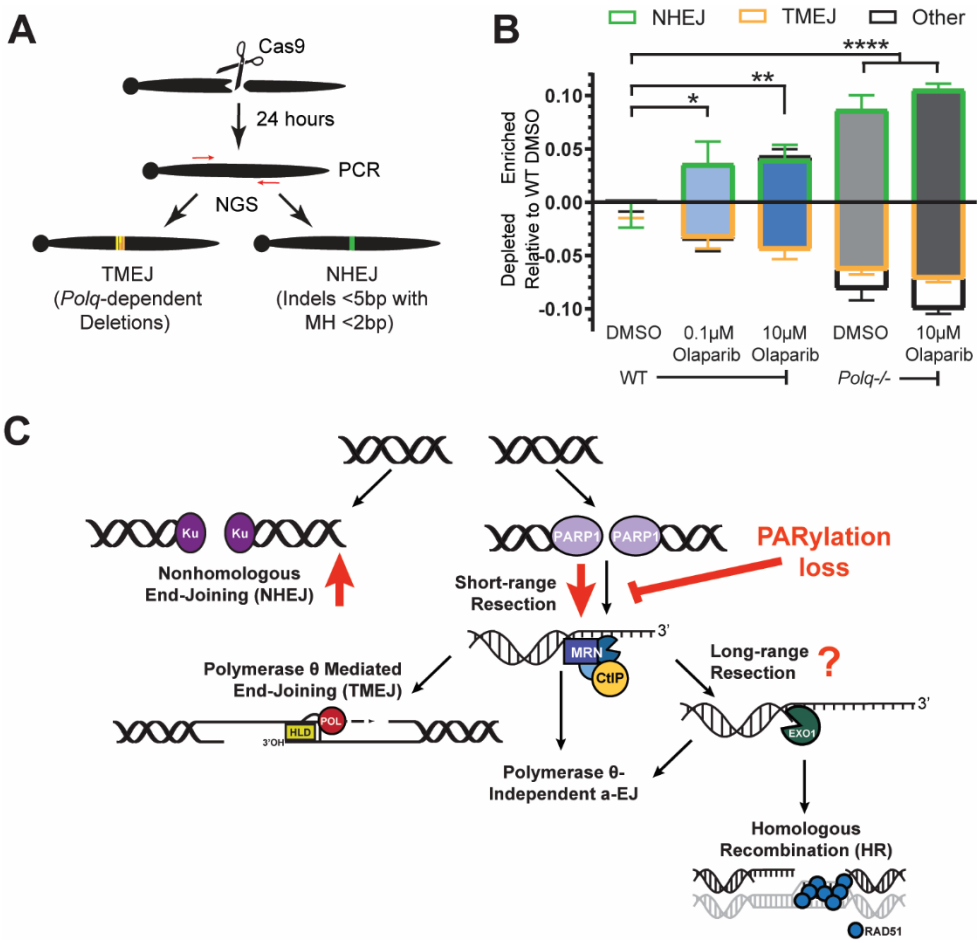

Figure 5 NHEJ compensates for the loss of TMEJ in the absence of PARP activity

A) Amplicon-based, next-generation sequencing (NGS) workflow used to characterize all TMEJ and NHEJ repair products. **B)** Percent of NHEJ (green outlined), TMEJ (orange outlined), and all other sequences (black outlined) enriched or depleted relative to DMSO-treated WT MEFs. NHEJ in DMSO-treated WT MEFs was 63%, TMEJ was 19%, and other was 17%. Data shown are mean ± SD (n=3). Statistical significance of differences, relative to WT DMSO, refers to NHEJ and TMEJ and was determined by two-way ANOVA (*p<0.05, **p<0.01, ****p<0.0001). *Polq-/-* MEFs treated with 10μM olaparib were the only condition significantly different from WT DMSO for other repair (p<0.01).

Supplementary Files

This is a list of supplementary files associated with this preprint. Click to download.

- LuedemanetalSupplementaryInformation.pdf